HHS Public Access

Author manuscript

Genes Cells. Author manuscript; available in PMC 2020 July 08.

Published in final edited form as:

Genes Cells. 2019 April ; 24(4): 307–317. doi:10.1111/gtc.12676.

Genetic interactions between Ror2 and Wnt9a, Ror1 and Wnt9a and Ror2 and Ror1: Phenotypic analysis of the limb skeleton and palate in compound mutants

Martina Weissenböck[1], **Richard Latham**[1], **Michiru Nishita**[2], **Lena Ingeborg Wolff**[3], **Hsin-Yi Henry Ho**[4], **Yasuhiro Minami**[2], **Christine Hartmann**[3]

[1]Research Institute of Molecular Pathology, Vienna, Austria

[2]Division of Cell Physiology, Department of Physiology and Cell Biology, Graduate School of Medicine, Kobe University, Kobe, Japan

[3]Department of Bone and Skeletal Research, Medical Faculty, Institute of Musculoskeletal Mediine, University of Münster, Münster, Germany

[4]Department of Cell Biology and Human Anatomy, University of California Davis School of Medicine, Davis, California

Abstract

Mutations in the human receptor tyrosine kinase ROR2 are associated with Robinow syndrome (RRS) and brachydactyly type B1. Amongst others, the shortened limb phenotype associated with RRS is recapitulated in *Ror2*$^{-/-}$ mutant mice. In contrast, *Ror1*$^{-/-}$ mutant mice are viable and show no limb phenotype. *Ror1*$^{-/-}$;*Ror2*$^{-/-}$ double mutants are embryonic lethal, whereas double mutants containing a hypomorphic *Ror1* allele (*Ror1*^{hyp}) survive up to birth and display a more severe shortened limb phenotype. Both orphan receptors have been shown to act as possible Wnt coreceptors and to mediate the Wnt5a signal. Here, we analyzed genetic interactions between the Wnt ligand, Wnt9a, and Ror2 or Ror1, as Wnt9a has also been implicated in skeletal development. *Wnt9a*$^{-/-}$ single mutants display a mild shortening of the long bones, whereas these are severely shortened in *Ror2*$^{-/-}$ mutants. *Ror2*$^{-/-}$;*Wnt9a*$^{-/-}$ double mutants displayed even more severely shortened long bones, and intermediate phenotypes were observed in compound *Ror2*;*Wnt9a* mutants. Long bones were also shorter in *Ror1*$^{hyp/hyp}$;*Wnt9a*$^{-/-}$ double mutants. In addition, *Ror1*$^{hyp/hyp}$;*Wnt9a*$^{-/-}$ double mutants displayed a secondary palate cleft phenotype, which was not present in the respective single mutants. Interestingly, 50% of compound mutant pups heterozygous for *Ror2* and homozygous mutant for *Ror1* also developed a secondary palate cleft phenotype.

Correspondence: Christine Hartmann, Department of Bone and Skeletal Research, Medical Faculty, Institute of Musculoskeletal Medicine, University of Münster, Münster, Germany. christine.hartmann@ukmuenster.de.

Communicated by: Kunihiro Matsumoto

AUTHOR CONTRIBUTIONS

Conceptualization: C.H.; Formal analyses and investigations: M.W., R.L., L.I.W., M.N.; Generation of material: H.H.; Writing—original draft preparation: C.H.; Writing—reviewing and editing: C.H, Y.M.; Supervision: C.H.

Keywords

chondrogenesis; endochondral ossification; limb skeleton; Ror1; Ror2; secondary cleft palate; Wnt9a

1 | INTRODUCTION

The two receptors Ror1 and Ror2 both interact with the Wnt5a ligand resulting in phosphorylation of the intracellular molecule dishevelled (Endo, Doi, Nishita, & Minami, 2012; Sato, Yamamoto, Sakane, Koyama, & Kikuchi, 2010). Mice lacking the orphan receptor Ror2 develop an embryonic skeletal dysplasia phenotype, with severe shortening of the long bones of the appendicular skeleton with a proximal–distal emphasis (DeChiara et al., 2000; Takeuchi et al., 2000). The related orphan receptor Ror1 appears to play a minor role in embryonic development. There are two different published *Ror1* alleles (Ho et al., 2012; Nomi et al., 2001). Homozygous mutant mice for either of the two *Ror1* alleles are viable, and their long bones develop normally until birth (Ho et al., 2012; Lyashenko et al., 2010). The two *Ror1* alleles differ as follows: The allele generated in the laboratory of Dr Minami (Nomi et al., 2001) produces two transcripts, one lacks exons 3 and 4 and possesses an early termination codon due to a frame-shift in exon 5. The other one lacks only exon 3 and produces a truncated Ror1 protein with a 96 a.a. deletion in its immunoglobulin (Ig)-like domain. The latter can still bind Wnt5a and subsequently induce phosphorylation of dishevelled, but to a lesser extent than the wild-type form (Qi, Okinaka, Nishita, & Minami, 2016). As such, this allele is predicted to be a hypomorphic allele (referred to in the following as $Ror1^{hyp}$). The second allele is a true protein null allele and was generated in the laboratory of Dr Greenberg (Ho et al., 2012). Double-mutant mice for both receptors, *Ror1* (hypomorphic as well as null allele) and *Ror2*, develop more a severe phenotype, which resembles the loss of the Wnt ligand, *Wnt5a*, in several aspects (Ho et al., 2012; Nomi et al., 2001). As double mutants with the *Ror1* null allele die at or soon after E13.5, long bone development has only been analyzed in the $Ror2^{-/-};Ror1^{hyp/hyp}$ mutants. Here, the skeletal dysplasia phenotype of the proximal long bones in the stylopod region, such as humerus (forelimb) and femur (hindlimb), is very pronounced and resembles that of $Wnt5a^{-/-}$ mutants. The more distal zeugopod elements (radius and ulna in the forelimb, and tibia and fibula in the hindlimb) and the autopod skeletal elements are affected to a lesser extent compared to $Wnt5a^{-/-}$ mutants (Nomi et al., 2001; Yamaguchi, Bradley, McMahon, & Jones, 1999; Yang, Topol, Lee, & Wu, 2003). Recessive mutations in human *ROR2* have been linked to Robinow syndrome that compromises amongst others dysmorphic facial features, short stature and brachydactyly (Afzal & Jeffery, 2003; Afzal et al., 2000; Brunetti-Pierri et al., 2008; Mehawej et al., 2012; Patton & Afzal, 2002; Tufan et al., 2005; van Bokhoven et al., 2000). In some patients, cleft lip/cleft palate phenotypes have been reported (Brunetti-Pierri et al., 2008; Roifman, Brunner, Lohr, Mazzeu, & Chitayat, 2015; Wang et al., 2012). $Ror2^{-/-}$ and $Wnt5a^{-/-}$ single-mutant mice, as well as $Ror2^{+/-};Wnt5a^{+/-}$ double-heterozygous-mutant mice, display a secondary cleft palate phenotype (He et al., 2008; Schwabe et al., 2004). Wnt5a and Ror2 have been associated with the noncanonical planar cell polarity Wnt-signaling pathway (Gao et al., 2011). Furthermore, it has been proposed that Wnt5a signaling through Ror2 counteracts the Wnt/β- catenin pathway (Mikels,

Minami, & Nusse, 2009; Mikels & Nusse, 2006; Topol et al., 2003; van Amerongen, Fuerer, Mizutani, & Nusse, 2012). Variations in numerous human WNT genes have also been associated with nonsyndromic cleft lip/cleft palate (Andrade Filho et al., 2011; Chiquet et al., 2008; Li et al., 2015; Menezes et al., 2010; Mostowska et al., 2012). Tetra-amelia is caused by homozygous mutations in the *WNT3* gene, a syndrome associated with the absence of all four limbs and craniofacial anomalies, amongst them cleft lip/cleft palate (Niemann et al., 2004). The aetiology of cleft lip/cleft palate is a multifactorial trait with complex interactions of genetic and environmental risk factors (Jugessur & Murray, 2005; Watkins, Meyer, Strauss, & Aylsworth, 2014).

Based on the phenotypic and molecular analyses, Ror2 has primarily been implicated as a receptor for Wnt5a in noncanonical signaling. In this study, we analyzed the potential genetic interaction between mutants for the Wnt ligand, Wnt9a (formerly known as Wnt14), and the Ror receptors, Ror1 and Ror2, focusing on the limb skeleton and the palate. Wnt9a is expressed in the developing joints and the perichondrium and has been implicated to play a role in joint development (Guo et al., 2004; Hartmann & Tabin, 2001). *Wnt9a* mutants display a slight shortening of the long bones at birth due to a temporal down-regulation in *Indian hedgehog* (*Ihh*) expression from E12.5 to E13.5 (Spater et al.., 2006). Skeletal preparations of $Ror2^{-/-}$;$Wnt9a^{-/-}$ double mutants showed an aggravated skeletal dysplasia phenotype of the long bones in the limbs, compared to $Ror2^{-/-}$ or $Ror2^{-/-}$;$Ror1^{hyp/hyp}$ mutants. In $Ror1^{hyp/hyp}$;$Wnt9a^{-/-}$ double mutants, the humerus displayed a pronounced shortening. In addition, we observed a secondary cleft palate phenotype in $Ror1^{hyp/hyp}$;$Wnt9a^{-/-}$ double mutants. Interestingly, this phenotype was also noticed in 50% of the examined $Ror2^{+/-}$;$Ror1^{hyp/hyp}$ compound mutants.

2 | RESULTS AND DISCUSSION

To address a possible interaction between the receptor Ror2 and the Wnt ligand, Wnt9a, we generated double and compound mutants. Loss of one copy of *Ror2* in the *Wnt9a* homozygous mutant background ($Ror2^{+/-}$;$Wnt9a^{-/-}$) slightly enhanced the $Wnt9a^{-/-}$ phenotype (Figure 1Ab,c). Likewise, the loss of one copy of *Wnt9a* in a *Ror2* mutant background ($Ror2^{-/-}$;$Wnt9a^{+/-}$) leads to a slightly increased shortening of the stylopod and zeugopod elements (reflected by the smaller alizarin red-positive regions) compared to the $Ror2^{-/-}$ mutant alone (compare Figure 1Ad,e). Skeletal preparations of the appendicular skeleton of $Ror2^{+/-}$;$Wnt9a^{+/-}$ double-heterozygous mutants, in contrast, resembled that of wild-type P0 specimens (data not shown). Yet, the $Ror2^{-/-}$;$Wnt9a^{-/-}$ double mutants displayed even more severely shortened long bones than the $Ror2^{-/-}$;$Ror1^{hyp/hyp}$ double mutants (Figure 1Af compared to Bc). Phenotypically, the limbs resembled the *Wnt5a* mutant phenotype in the stylopod (humerus, femur) and zeugopod (radius and ulna, tibia and fibula), but not in the autopod and digit region (Figure 1Af) (Yamaguchi et al., 1999). Particularly, the endochondral ossification process in the zeugopods of $Ror2^{-/-}$;$Wnt9a^{-/-}$ double mutants was much more delayed than in $Ror2^{-/-}$;$Ror1^{hyp/hyp}$ double mutants as the mineralized, alizarin red-positive region was absent in the radius and severely reduced in the ulna (asterisks, Figure 1Af compare to Bc). The phenotypic alterations in the hindlimb were similar (data not shown). $Ror1^{hyp/hyp}$ mutants show no skeletal phenotype with respect to their long bones at birth (Figure 1Cb) (Lyashenko et al., 2010), and $Wnt9a^{-/-}$ mutants

display only a slight shortening (Figure 1Cc) (Spater et al., 2006). Given our results that lack of *Wnt9a* exaggerated the *Ror2* mutant phenotype, we asked whether decreased Ror1 signaling would affect the *Wnt9a* skeletal phenotype. Skeletal preparations of $Ror1^{hyp/hyp}$;$Wnt9a^{-/-}$ double mutants showed a pronounced shortening of about 30% of the mineralized part of the long bones particular in the stylopod (humerus, femur) (Figure 1Ca,d). Long bone growth was similar to wild type in $Ror1^{hyp/+}$;$Wnt9a^{+/-}$ double-heterozygous mutants (Figure 1 Ca and data not shown). Hence, given our phenotypic analysis of the limb skeleton, we conclude that the downstream pathways of Ror2 and Wnt9a, and Ror1 and Wnt9a converge and act synergistically on the process of chondrocyte maturation.

Based on evidence from the literature, we hypothesized that the two signaling pathways Ror2 and Wnt9a might possibly converge at the level of *Ihh* regulation. We have shown before that *Wnt9a* temporarily regulates *Ihh* expression at around E12.5-E13.5 and at least at E15.5 *Ihh* is severely reduced in the stylopod of *Ror2* mutants (Schwabe et al., 2004; Spater et al., 2006). In order to further investigate this, we carried out a temporal expression analysis from E11.5 to E15.5 on $Ror2^{-/-}$ and $Ror2^{-/-};Wnt9a^{-/-}$ mutant limbs. Compared to controls, *Ihh* expression occurred normally in the $Ror2^{-/-}$ single mutant at E11.5, but it was down-regulated at E12.5-E13.5 in the humerus (Figure 2A). At E14.5, *Ihh* expression was detected in 50% of the *Ror2* mutant stylopods analyzed and absent in the other 50% ($n = 4$; Figure 2A). Similar to the $Ror2^{-/-}$ mutants, the onset of *Ihh* expression also occurred normally at E11.5 in the $Ror2^{-/-};Wnt9a^{-/-}$ double mutants (Figure 2B). Yet, at E13.5 *Ihh* expression was even further reduced than in the *Ror2* mutant (compare Figure 2A,C). Histologically, no signs of hypertrophy were detected on alcian blue-stained sections, and accordingly, no signals were detected for the *Col10a1* in situ probes normally marking hypertrophic chondrocyte differentiation (Figure 2C). *Ihh* expression levels recovered to normal levels in the $Wnt9a^{-/-}$ at E14.5 (Spater et al., 2006) and in the $Ror2^{-/-}$ single mutants at E15.5; however, the *Ihh* expression domains were not yet fully separated in the $Ror2^{-/-}$ mutants (Figure 2Db′). Along with the recovery of *Ihh* expression, hypertrophic chondrocyte differentiation was detected in the $Ror2^{-/-}$ mutants by morphology and using the molecular marker *Col10a1* (Figure 2Db,b″). In contrast, in the $Ror2^{-/-};Wnt9a^{-/-}$ double mutants *Ihh* was only very weakly expressed at E15.5 (Figure 2Dd′). In addition, histologically no signs of hypertrophy could be detected, and accordingly, *Col10a1* expression was absent in E15.5 double-mutant limbs (Figure 2Dd,d″). Alcian blue/von Kossa staining on sections from humeri of newborns (P0) showed that bone marrow formation had just started in the humeri of $Ror2^{-/-};Wnt9a^{-/-}$ double mutants, compared to wild-type, $Ror2^{-/-}$, and compound $Ror2^{-/-};Wnt9a^{+/-}$ mutants (Figure 3Aa–d). In accordance with the results from the whole skeletal stainings, chondrocyte maturation was even more delayed in the radius and ulna of the $Ror2^{-/-};Wnt9a^{-/-}$ double mutants based on alcian blue/von Kossa staining and *Col10a1* in situ hybridization (Figure 3Bd,d′) compared to compound $Ror2^{-/-};Wnt9a^{+/-}$ (Figure 3Bc,c'), $Ror2^{-/-}$ single (Figure 3Bb,b') or double-heterozygous $Ror2^{+/-};Wnt9a^{+/-}$ mutant newborns (Figure 3Ba,a'). The latter developed as the wild-type newborns (data not shown). Marker analysis for hypertrophic chondrocytes (*Col10a1*) and osteoblasts (*collagen 1a1* (*Col1a1*) and *osteocalcin* (*Oc*)) was carried out on P0 humeri of the different mutants. In $Ror2^{-/-};Wnt9a^{-/-}$ double-mutant humeri, *Col10a1*

was expressed (Figure 3Cd). Yet, in contrast to compound *Ror2*$^{-/-}$;*Wnt9a*$^{+/-}$ (Figure 3Cc), *Ror2*$^{-/-}$ single mutants (Figure 3Cb), or *Ror2*$^{+/-}$;*Wnt9a*$^{+/-}$ double-heterozygous mutants (Figure 3Ca) the *Col10a1* expression domains in the *Ror2*$^{-/-}$;*Wnt9a*$^{-/-}$ double-mutant humeri were not fully separated (Figure 3Cd). Expression of the osteoblast marker *Col1a1* was reduced and restricted to the bone collar and the asymmetrically occurring bone marrow-forming region in the *Ror2*$^{-/-}$;*Wnt9a*$^{-/-}$ double mutants (Figure 3Cd′). Furthermore, no *Oc*-positive cells were detected in the bone collar region of double-mutant humeri (Figure 3Cd″), whereas they were present in the compound *Ror2*$^{-/-}$;*Wnt9a*$^{+/-}$ (Figure 3Cc″), the *Ror2*$^{-/-}$ single (Figure 3Cb″) and the *Ror2*$^{-/-}$;*Wnt9a*$^{+/-}$ mutants (Figure 3Ca″). This shows that along with chondrocyte maturation, osteoblast maturation is severely delayed in the *Ror2*$^{-/-}$;*Wnt9a*$^{-/-}$ double mutants. Thus, in summary, our data suggest that Wnt9a signaling can in part compensate for the loss of Ror2 signaling and that both signaling pathways converge at the level of *Ihh* regulation.

In *Ror1*$^{hyp/hyp}$ mutants, no embryonic phenotype has been reported with regard to long bone growth (Lyashenko et al., 2010; Nomi et al., 2001). The *Ror1* null allele mutants have not yet been characterized in detail, but they are viable and do not display any obvious morphological phenotypes at birth (Ho et al., 2012). As such, compensatory mechanisms mediated by Ror2 might account for the lack of an embryonic phenotype of *Ror1* mutants. Similar to the previous publication showing a compensatory mechanism between Ror1 and Ror2 (Nomi et al., 2001), our data suggest that Ror1 signaling may in part compensate for the loss of *Wnt9a*, as the skeletal preparations of the limbs showed a more severe phenotype in the double mutants compared to the single mutants (Figure 1C). Furthermore, when examining the whole-mount skeletal preparations a cleft secondary palate phenotype was observed in the *Ror1*$^{hyp/hyp}$;*Wnt9a*$^{-/-}$ mutants (n = 3) (Figure 4A). Neither *Ror1* mutants nor *Wnt9a*$^{-/-}$ single mutants display a cleft palate phenotype (Ho et al., 2012; Lyashenko et al., 2010; Nomi et al., 2001; Spater et al., 2006). Yet, in zebrafish Wnt9a is required for palatal extension during palatal morphogenesis and an incompletely penetrant cleft palate phenotype was reported in mouse mutants lacking the closely related family member Wnt9b (formerly known as Wnt15) (Carroll, Park, Hayashi, Majumdar, & McMahon, 2005; Curtin, Hickey, Kamel, Davidson, & Liao, 2011; Dougherty et al., 2013; Jin, Han, Taketo, & Yoon, 2012). In addition, the recessive knockout *Wnt9b* allele is allelic to the *clf1* locus of the A/WySn strain that models the human defect (Juriloff, Harris, McMahon, Carroll, & Lidral, 2006). Further analysis of the *clf1* region uncovered that an intracisternal A particle (IAP) retrotransposon was inserted near the *Wnt9b* gene. Associated epigenetic alterations at the mouse *Wnt9b* gene locus lead to altered *Wnt9b* expression levels and contribute to the phenotype of the A/WySn strain (Juriloff, Harris, Mager, & Gagnier, 2014). Polymorphisms in the human *WNT9B* homologue have also been associated with nonsyndromic cleft lip/cleft palate (Fontoura, Silva, Granjeiro, & Letra, 2015). Thus, our analysis uncovered a potential redundant role for *Wnt9a* in secondary palate formation.

In the course of analyzing the *Ror2;Ror1*^{hyp} compound mutants, we noticed that approximately 50% (n = 9/19) of the *Ror2*$^{+/-}$;*Ror1*$^{hyp/hyp}$ mutants displayed a cleft secondary palate phenotype (Figure 4B–D). The phenotype is not linked to the sex of the mice. Interestingly, it has been proposed that the cleft secondary palate phenotype in the *Ror2*$^{-/-}$ mutants is in part due to a down-regulation of the expression of another hedgehog

family member, *sonic hedgehog* (*Shh*), in the medial edge epithelium and altered cell proliferation in the mesenchyme of the anterior palate particular in the nasal aspect (He et al., 2008). Ror2 has been implicated to act as the receptor for Wnt5a in palate shelf formation. Yet, the phenotype of the *Ror2* mutant is less severe than that of the *Wnt5a* mutant with respect to the posterior region (He et al., 2008). Our finding in the compound mutants suggests that in analogy to the situation in the limb Ror1 might act as a receptor for Wnt5a in addition to Ror2 during palatogenesis. Given that two transcripts can be generated from the hypomorphic *Ror1* allele, one producing a truncated Ror1 protein and one producing no protein, it is possible that the $Ror2^{+/-};Ror1^{hyp/hyp}$ mutants with and without a cleft secondary palate phenotype differ in their amount of partially functional Ror1 protein present. Further reduction of signaling by removal of the second copy of *Ror2* did not lead to a worsening of the phenotype—at least at the level of skeletal preparations $Ror2^{-/-};Ror1^{hyp/hyp}$ mutant heads were indistinguishable from those of $Ror2^{-/-};Ror1^{+/+}$ or $Ror2^{+/-};Ror1^{hyp/hyp}$ mutants (data not shown). In addition, we analyzed the heads of E13.5 $Ror2^{+/-};Ror1^{-/-}$, control and $Ror2^{-/-}$ embryos ($n = 2–3$). Although defects in palatal shelf fusion cannot be detected morphologically at this stage, the size of the $Ror2^{+/-};Ror1^{-/-}$ mutant palatal shelves was on average smaller than that of controls (genotypes: $Ror2^{+/+};Ror1^{+/-}$ and $Ror2^{+/-};Ror1^{+/-}$) and of $Ror2^{-/-}$ mutant embryos (see Figure 4F). Size measurements could only be carried out on two samples of each genotype; hence, we can currently only state that there is a clear trend for a size reduction of the anterior palate in the $Ror2^{+/-};Ror1^{-/-}$ mutants in comparison with the controls and $Ror2^{-/-}$ mutants. In the latter, the size appeared to be increased in the anterior palate compared to controls and $Ror2^{+/-};Ror1^{-/-}$ mutants. This is in agreement with the previous finding of increased cell proliferation in the anterior palate in *Ror2* as well as *Wnt5a* mutants (He et al., 2008). This suggests that the mechanism of the cleft secondary palate phenotypes in the $Ror2^{+/-};Ror1^{hyp/hyp}$ compound and probably also in the $Ror1^{hyp/hyp};Wnt9a^{-/-}$ mutants may be different from that in *Ror2* or *Wnt5a* mutants. Future studies are necessary to examine this. Skeletal preparations of $Ror2^{+/-};Wnt9a^{-/-}$ mice do not display a cleft secondary palate phenotype, and the heads of $Ror2^{-/-};Wnt9a^{-/-}$ double mutants were indistinguishable from those of $Ror2^{-/-};Wnt9a^{+/+}$ mutants (data not shown). Thus, in contrary to what we have observed in the appendicular skeleton there appears to be no genetic interaction between Ror2 and Wnt9a signaling with respect to secondary palate formation.

According to a previous publication, *Ror2* is expressed in an anterior to posterior graded fashion in the epithelium and mesenchyme of the palate, with the anterior mesenchymal domain being restricted to the medial region (He et al., 2008). In our hands, at E13.5, *Ror2* expression was restricted to the mesenchyme of the palatal shelf in a nongraded fashion and is expressed highest underneath the ectoderm (Figure 4E). *Ror1* expression was also detected in the palatal mesenchyme (Figure 4E). Yet, no distinct *Wnt9a* expression was detected in the palatal shelf at E13.5 (Figure 4E). In the anterior-most region *Wnt9a* was weakly expressed in the incisor region (Figure 4E). Interestingly, *Wnt9b* expression is also not detected in the secondary palate throughout its development, but *Wnt9b* is expressed earlier in the midfacial ectoderm (Lan et al., 2006).

Co-immunoprecipitation of extracts from HEK cells co-expressing Wnts and Ror1 or Ror2 showed that Wnt9a interacted with both Ror receptors Ror1 and Ror2, as did Wnt3a, Wnt5a

and Wnt9b (Figure 5A). As in the *Ror1*^{hyp} mice, a truncated protein lacking the immunoglobulin (Ig)-like domain is still produced, we tested whether Wnt9a, like Wnt5a, can still interact with the Ror1ΔIg form. Indeed, Wnt9a, like Wnt5a, was able to bind to the Ror1ΔIg protein, but both Wnt ligands failed to interact with Ror1 and Ror2 proteins lacking the cysteine-rich, extracellular domain (ΔCRD) (Figure 5B,C).

Taken together, our results suggest that mutations in *WNT9A* and *ROR1* may be additional risk factors for nonsyndromic cleft lip/cleft palate and combinatorial modulators of long bone growth. Mutations in these genes may not easily be identified by genome-wide association studies as risk factors, because this would require sufficiently large pedigrees for statistical power or combining GWAS with other analytical methods to detect such compound genetic risk factors (Mooney, Nigg, McWeeney, & Wilmot, 2014; Weiss et al., 2012; Wittkowski et al., 2013).

3 | EXPERIMENTAL PROCEDURES

3.1 | Mouse husbandry

The generation of the *Ror1*, *Ror2* and *Wnt9a* mutant alleles has been previously described (Ho et al., 2012; Nomi et al., 2001; Spater et al., 2006; Takeuchi et al., 2000). *Ror1* and *Ror2* strains were maintained on a C57BL/6J background. Mutants were generated by intercrosses of heterozygous mice, or through breeding of homozygous males with heterozygous females to increase the number of mutant off-spring. Genotyping of newborn mice and embryos by PCR was carried out as previously described for *Ror1* (Lyashenko et al., 2010) and *Ror2* (Schwabe et al., 2004), and for *Wnt9a*, the following primer sequences were used: Wnt9a_For1: 5- GCGAGGTAAGCTCTGCTTGCCTCC-3′, Wnt9a_For2: 5′-GCTCTGATGCCGCCGTGTTCC-3′, Wnt9a_Rev: 5′-CGA GGCTTTCGGTCAAAGCTGATGG-3′ amplifying a 100-bp wild-type and an 1,100-bp mutant allele. The E13.5 $Ror2^{+/+};Ror1^{+/-}$ (control), $Ror2^{+/-};Ror1^{-/-}$ and $Ror2^{-/-};Ror1^{+/+}$ embryos were provided by H. Ho Lab. To generate double and compound mutant embryos and newborns, the respective double-heterozygous animals were interbred using timed matings.

3.2 | Whole-mount skeletal preparations

Newborn pups (P0) and embryos were skinned, eviscerated and fixed in 95% EtOH. Skeletons were stained with alizarin red and alcian blue for mineralized and cartilaginous regions, respectively (McLeod, 1980), and cleared through serial processing with 1% KOH, 1% KOH:glycerol (3:1; 1:1; 1:3) into pure glycerol.

3.3 | Histology and in situ hybridization

For histology and section in situ hybridizations, embryos and newborns were fixed overnight in 4% PFA/PBS and dehydrated to 100% EtOH. Newborns were skinned before fixation. Limbs were removed in 75% EtOH and processed into paraffin. Mutant and wild-type limbs were embedded into the same paraffin block, and alternating sections at 6 μm were generated. Sections processed for van Kossa/alcian blue stainings were deparaffinized and rehydrated into H_2O. Mineralization was visualized by incubation of sections in 2% silver

nitrate solution under light exposure (60-W bulb) for 1 hr. For subsequent cartilage matrix visualization, sections were washed with 1% acetic acid and stained for 15 min in alcian blue staining solution (20 mg alcian blue in 70 ml EtOH, 30 ml acetic acid, filtered). Before dehydration and mounting with DPX (Sigma), the tissue was counterstained with eosin.

Nonradioactive section in situ hybridizations using digoxigenin-labeled RNA probes were carried out according to Murtaugh, Zeng, Chyung, and Lassar (2001). Probes for *Ihh*, *Col10a1*, *Col2a1*, *Col1a1*, *Osc* (Hill, Spater, Taketo, Birchmeier, & Hartmann, 2005), *Ror2*, *Ror1* (Oishi et al., 1999), and *Wnt9a* (Kahn et al., 2009) have been previously published and are available on request.

3.4 |

Plasmids encoding Flag-tagged mouse Ror1 and Ror2 and their derivative deletion mutants were constructed as described (Matsuda et al., 2003; Oishi et al., 2003; Qi et al., 2016). Wnt9a and Wnt5a hemagglutinin (HA)-tagged expression plasmids were generated by inserting the coding regions of Wnt9a and Wnt5a first into the phCMV3 vector (Genlantis) containing a C-terminal HA-tag. Subsequently, the tagged cDNAs were cloned into a modified pCAAGS vector (Niwa, Yamamura, & Miyazaki, 1991) containing, in addition, a PGK-neo cassette for selection in mammalian cells.

3.5 | Co-immunoprecipitation

HEK293T cells were cultured in DMEM containing 10% (v/v) fetal calf serum and transiently cotransfected with Wnt-HA and Ror-Flag expression plasmids using Lipofectamine 2000 (Life Technologies) according to the manufacturer's instruction. At 24 hr after transfection, cells were solubilized with lysis buffer (50 mM Tris-HCl (pH 7.5), 150 mM NaCl, 5 mM EDTA, 0.5% (v/v) NP-40, 50 mM NaF, 1 mM Na_3VO_4, 10 μg/ml leupeptin, 10 μg/ml aprotinin, 0.25 mM pAPMSF) and centrifuged at 12,000 *g* for 20 min. Whole cell lysates were subjected to immunoprecipitation with an anti-HA antibody (16B12, Covance), followed by Western blotting with anti-Flag (1E6, Wako) and anti-HA (3F10, Roche) antibodies.

Funding Information

The majority of the work was carried out at the Institute of Molecular Pathology (IMP), Vienna Austria, and was supported by Boehringer Ingelheim funding the IMP. L.I.W. is supported by a grant from the German Federal Ministry of Education and Science (01EC1408E), as part of the OVERLOAD-Prev-OP consortium. H.H. is supported by a National Institutes of Health grant #1R35GM119574. The founding organizations had no role in the study design, data collection and analysis, decision to publish or preparation of the manuscript.

REFERENCES

Afzal AR, & Jeffery S (2003). One gene, two phenotypes: ROR2 mutations in autosomal recessive Robinow syndrome and autosomal dominant brachydactyly type B. Human Mutation, 22(1), 1–11. 10.1002/humu.10233 [PubMed: 12815588]

Afzal AR, Rajab A, Fenske CD, Oldridge M, Elanko N, Ternes-Pereira E, … Jeffery S (2000). Recessive Robinow syndrome, allelic to dominant brachydactyly type B, is caused by mutation of ROR2. Nature Genetics, 25(4), 419–422. 10.1038/78107 [PubMed: 10932186]

Andrade Filho PA, Letra A, Cramer A, Prasad J. l., Garlet GP, Vieira AR, … Menezes R (2011). Insights from studies with oral cleft genes suggest associations between WNT-pathway genes and

risk of oral cancer. Journal of Dental Research, 90(6), 740–746. 10.1177/0022034511401622 [PubMed: 21393552]

Brunetti-Pierri N, Del Gaudio D, Peters H, Justino H, Ott CE, Mundlos S, & Bacino CA (2008). Robinow syndrome: Phenotypic variability in a family with a novel intragenic ROR2 mutation. American Journal of Medical Genetics. Part A, 146A(21), 2804–2809. 10.1002/ajmg.a.32530 [PubMed: 18831060]

Carroll TJ, Park JS, Hayashi S, Majumdar A, & McMahon AP (2005). Wnt9b plays a central role in the regulation of mesenchymal to epithelial transitions underlying organogenesis of the mammalian urogenital system. Developmental Cell, 9(2), 283–292. 10.1016/j.devcel.2005.05.016 [PubMed: 16054034]

Chiquet BT, Blanton SH, Burt A, Ma D, Stal S, Mulliken JB, & Hecht JT (2008). Variation in WNT genes is associated with nonsyndromic cleft lip with or without cleft palate. Human Molecular Genetics, 17(14), 2212–2218. 10.1093/hmg/ddn121 [PubMed: 18413325]

Curtin E, Hickey G, Kamel G, Davidson AJ, & Liao EC (2011). Zebrafish wnt9a is expressed in pharyngeal ectoderm and is required for palate and lower jaw development. Mechanisms of Development, 128(1–2), 104–115. 10.1016/j.mod.2010.11.003 [PubMed: 21093584]

DeChiara TM, Kimble RB, Poueymirou WT, Rojas J, Masiakowski P, Valenzuela DM, & Yancopoulos GD (2000). Ror2, encoding a receptor-like tyrosine kinase, is required for cartilage and growth plate development. Nature Genetics, 24(3), 271–274. 10.1038/73488 [PubMed: 10700181]

Dougherty M, Kamel G, Grimaldi M, Gfrerer L, Shubinets V, Ethier R, … Liao EC (2013). Distinct requirements for wnt9a and irf6 in extension and integration mechanisms during zebrafish palate morphogenesis. Development, 140(1), 76–81. 10.1242/dev.080473 [PubMed: 23154410]

Endo M, Doi R, Nishita M, & Minami Y (2012). Ror family receptor tyrosine kinases regulate the maintenance of neural progenitor cells in the developing neocortex. Journal of Cell Science, 125(Pt 8), 2017–2029. 10.1242/jcs.097782 [PubMed: 22328498]

Fontoura C, Silva RM, Granjeiro JM, & Letra A (2015). Association of WNT9B gene polymorphisms with nonsyndromic cleft lip with or without cleft palate in Brazilian nuclear families. Cleft Palate-Craniofacial Journal, 52(1), 44–48. 10.1597/13-146 [PubMed: 24437584]

Gao BO, Song H, Bishop K, Elliot G, Garrett L, English MA, … Yang Y (2011). Wnt signaling gradients establish planar cell polarity by inducing Vangl2 phosphorylation through Ror2. Developmental Cell, 20(2), 163–176. 10.1016/j.devcel.2011.01.001 [PubMed: 21316585]

Guo X, Day TF, Jiang X, Garrett-Beal L, Topol L, & Yang Y (2004). Wnt/beta-catenin signaling is sufficient and necessary for synovial joint formation. Genes & Development, 18(19), 2404–2417. 10.1101/gad.1230704 [PubMed: 15371327]

Hartmann C, & Tabin CJ (2001). Wnt-14 plays a pivotal role in inducing synovial joint formation in the developing appendicular skeleton. Cell, 104(3), 341–351. 10.1016/S0092-8674(01)00222-7 [PubMed: 11239392]

He F, Xiong W, Yu X, Espinoza-Lewis R, Liu C, Gu S, … Chen Y (2008). Wnt5a regulates directional cell migration and cell proliferation via Ror2-mediated noncanonical pathway in mammalian palate development. Development, 135(23), 3871–3879. 10.1242/dev.025767 [PubMed: 18948417]

Hill TP, Spater D, Taketo MM, Birchmeier W, & Hartmann C (2005). Canonical Wnt/beta-catenin signaling prevents osteoblasts from differentiating into chondrocytes. Developmental Cell, 8(5), 727–738. 10.1016/j.devcel.2005.02.013 [PubMed: 15866163]

Ho H-Y-H, Susman MW, Bikoff JB, Ryu YK, Jonas AM, Hu L, … Greenberg ME (2012). Wnt5a-Ror-Dishevelled signaling constitutes a core developmental pathway that controls tissue morphogenesis. Proceedings of the National Academy of Sciences, 109(11), 4044–4051. 10.1073/pnas.1200421109

Jin YR, Han XH, Taketo MM, & Yoon JK (2012). Wnt9b-dependent FGF signaling is crucial for outgrowth of the nasal and maxillary processes during upper jaw and lip development. Development, 139(10), 1821–1830. 10.1242/dev.075796 [PubMed: 22461561]

Jugessur A, & Murray JC (2005). Orofacial clefting: Recent insights into a complex trait. *Current Opinion in Genetics &* Development, 15(3), 270–278. 10.1016/j.gde.2005.03.003

Juriloff DM, Harris MJ, Mager DL, & Gagnier L (2014). Epigenetic mechanism causes Wnt9b deficiency and nonsyndromic cleft lip and palate in the A/WySn mouse strain. *Birth Defects Research Part A*: Clinical and Molecular Teratology, 100(10), 772–788. 10.1002/bdra.23320 [PubMed: 25257647]

Juriloff DM, Harris MJ, McMahon AP, Carroll TJ, & Lidral AC (2006). Wnt9b is the mutated gene involved in multifactorial nonsyndromic cleft lip with or without cleft palate in A/WySn mice, as confirmed by a genetic complementation test. Birth Defects Research Part A: Clinical and Molecular Teratology, 76(8), 574–579. 10.1002/bdra.20302 [PubMed: 16998816]

Kahn J, Shwartz Y, Blitz E, Krief S, Sharir A, Breitel DA, … Zelzer E (2009). Muscle contraction is necessary to maintain joint progenitor cell fate. Developmental Cell, 16(5), 734–743. 10.1016/j.devcel.2009.04.013 [PubMed: 19460349]

Lan YU, Ryan RC, Zhang Z, Bullard SA, Bush JO, Maltby KM, … Jiang R (2006). Expression of Wnt9b and activation of canonical Wnt signaling during midfacial morphogenesis in mice. Developmental Dynamics, 235(5), 1448–1454. 10.1002/dvdy.20723 [PubMed: 16496313]

Li Q, Kim Y, Suktitipat B, Hetmanski JB, Marazita ML, Duggal P, … Bailey-Wilson JE (2015). Gene-gene interaction among WNT genes for oral cleft in trios. Genetic Epidemiology, 39(5), 385–394. 10.1002/gepi.21888 [PubMed: 25663376]

Lyashenko N, Weissenbock M, Sharir A, Erben RG, Minami Y, & Hartmann C (2010). Mice lacking the orphan receptor ror1 have distinct skeletal abnormalities and are growth retarded. Developmental Dynamics, 239(8), 2266–2277. 10.1002/dvdy.22362 [PubMed: 20593419]

Matsuda T, Suzuki H, Oishi I, Kani S, Kuroda Y, Komori T, … Minami Y (2003). The receptor tyrosine kinase Ror2 associates with the melanoma-associated antigen (MAGE) family protein Dlxin-1 and regulates its intracellular distribution. Journal of Biological Chemistry, 278(31), 29057–29064. 10.1074/jbc.M302199200 [PubMed: 12754255]

McLeod MJ (1980). Differential staining of cartilage and bone in whole mouse fetuses by alcian blue and alizarin red S. Teratology, 22(3), 299–301. 10.1002/tera.1420220306 [PubMed: 6165088]

Mehawej C, Chouery E, Maalouf D, Baujat G, Le Merrer M, Cormier-Daire V, & Megarbane A (2012). Identification of a novel causative mutation in the ROR2 gene in a Lebanese family with a mild form of recessive Robinow syndrome. European Journal of Medical Genetics, 55(2), 103–108. 10.1016/j.ejmg.2011.11.003 [PubMed: 22178368]

Menezes R, Letra A, Kim AH, Küchler EC, Day A, Tannure PN, … Vieira AR (2010). Studies with Wnt genes and nonsyndromic cleft lip and palate. Birth Defects Research Part A: Clinical and Molecular Teratology, 88(11), 995–1000. 10.1002/bdra.20720 [PubMed: 20890934]

Mikels A, Minami Y, & Nusse R (2009). Ror2 receptor requires tyrosine kinase activity to mediate Wnt5A signaling. Journal of Biological Chemistry, 284(44), 30167–30176. 10.1074/jbc.M109.041715 [PubMed: 19720827]

Mikels AJ, & Nusse R (2006). Purified Wnt5a protein activates or inhibits beta-catenin-TCF signaling depending on receptor context. PLoS Biology, 4(4), e115 10.1371/journal.pbio.0040115 [PubMed: 16602827]

Mooney MA, Nigg JT, McWeeney SK, & Wilmot B (2014). Functional and genomic context in pathway analysis of GWAS data. Trends in Genetics, 30(9), 390–400. 10.1016/j.tig.2014.07.004 [PubMed: 25154796]

Mostowska A, Hozyasz KK, Biedziak B, Wojcicki P, Lianeri M, & Jagodzinski PP (2012). Genotype and haplotype analysis of WNT genes in nonsyndromic cleft lip with or without cleft palate. European Journal of Oral Sciences, 120(1), 1–8. 10.1111/j.1600-0722.2011.00938.x [PubMed: 22288914]

Murtaugh LC, Zeng L, Chyung JH, & Lassar AB (2001). The chick transcriptional repressor Nkx3.2 acts downstream of Shh to promote BMP-dependent axial chondrogenesis. Developmental Cell, 1(3), 411–422. [PubMed: 11702952]

Niemann S, Zhao C, Pascu F, Stahl U, Aulepp U, Niswander L, … Müller U (2004). Homozygous WNT3 mutation causes tetra-amelia in a large consanguineous family. American Journal of Human Genetics, 74(3), 558–563. 10.1086/382196 [PubMed: 14872406]

Niwa H, Yamamura K, & Miyazaki J (1991). Efficient selection for high-expression transfectants with a novel eukaryotic vector. Gene, 108(2), 193–199. 10.1016/0378-1119(91)90434-D [PubMed: 1660837]

Nomi M, Oishi I, Kani S, Suzuki H, Matsuda T, Yoda A, … Minami Y (2001). Loss of mRor1 enhances the heart and skeletal abnormalities in mRor2-deficient mice: Redundant and pleiotropic functions of mRor1 and mRor2 receptor tyrosine kinases. Molecular and Cellular Biology, 21(24), 8329–8335. 10.1128/MCB.21.24.8329-8335.2001 [PubMed: 11713269]

Oishi I, Suzuki H, Onishi N, Takada R, Kani S, Ohkawara B, … Minami Y (2003). The receptor tyrosine kinase Ror2 is involved in noncanonical Wnt5a/JNK signalling pathway. Genes to Cells, 8(7), 645–654. 10.1046/j.1365-2443.2003.00662.x [PubMed: 12839624]

Oishi I, Takeuchi S, Hashimoto R, Nagabukuro A, Ueda T, Liu Z-J, … Minami Y (1999). Spatio-temporally regulated expression of receptor tyrosine kinases, mRor1, mRor2, during mouse development: Implications in development and function of the nervous system. Genes to Cells, 4(1), 41–56. 10.1046/j.1365-2443.1999.00234.x [PubMed: 10231392]

Patton MA, & Afzal AR (2002). Robinow syndrome. Journal of Medical Genetics, 39(5), 305–310. 10.1136/jmg.39.5.305 [PubMed: 12011143]

Qi X, Okinaka Y, Nishita M, & Minami Y (2016). Essential role of Wnt5a-Ror1/Ror2 signaling in metanephric mesenchyme and ureteric bud formation. Genes to Cells, 21(4), 325–334. 10.1111/gtc.12342 [PubMed: 26840931]

Roifman M, Brunner H, Lohr J, Mazzeu J, & Chitayat D (2015). Autosomal dominant robinow syndrome In Pagon RA, Adam MP, Ardinger HH, Bird TD, Dolan CR, Fong CT, Smith RJH, & Stephens K (Eds.), GeneReviews(R). Seattle, WA: University of Washington, Seattle.

Sato A, Yamamoto H, Sakane H, Koyama H, & Kikuchi A (2010). Wnt5a regulates distinct signalling pathways by binding to Frizzled2. EMBO Journal, 29(1), 41–54. 10.1038/emboj.2009.322 [PubMed: 19910923]

Schwabe GC, Trepczik B, Suring K, Brieske N, Tucker AS, Sharpe PT, … Mundlos S (2004). Ror2 knockout mouse as a model for the developmental pathology of autosomal recessive Robinow syndrome. Developmental Dynamics, 229(2), 400–410. 10.1002/dvdy.10466 [PubMed: 14745966]

Spater D, Hill TP, O'Sullivan RJ, Gruber M, Conner DA, & Hartmann C (2006). Wnt9a signaling is required for joint integrity and regulation of Ihh during chondrogenesis. Development, 133(15), 3039–3049. 10.1242/dev.02471 [PubMed: 16818445]

Takeuchi S, Takeda K, Oishi I, Nomi M, Ikeya M, Itoh K, … Minami Y (2000). Mouse Ror2 receptor tyrosine kinase is required for the heart development and limb formation. Genes to Cells, 5(1), 71–78. 10.1046/j.1365-2443.2000.00300.x [PubMed: 10651906]

Topol L, Jiang X, Choi H, Garrett-Beal L, Carolan PJ, & Yang Y (2003). Wnt5a inhibits the canonical Wnt pathway by promoting GSK-3-independent beta-catenin degradation. Journal of Cell Biology, 162(5), 899–908. 10.1083/jcb.200303158 [PubMed: 12952940]

Tufan F, Cefle K, Türkmen S, Türkmen A, Zorba U, Dursun M, … Horn D (2005). Clinical and molecular characterization of two adults with autosomal recessive Robinow syndrome. American Journal of Medical Genetics Part A, 136(2), 185–189. 10.1002/ajmg.a.30785 [PubMed: 15952209]

van Amerongen R, Fuerer C, Mizutani M, & Nusse R (2012). Wnt5a can both activate and repress Wnt/beta-catenin signaling during mouse embryonic development. Developmental Biology, 369(1), 101–114. 10.1016/j.ydbio.2012.06.020 [PubMed: 22771246]

van Bokhoven H, Celli J, Kayserili H, van Beusekom E, Balci S, Brussel W, … Brunner HG (2000). Mutation of the gene encoding the ROR2 tyrosine kinase causes autosomal recessive Robinow syndrome. Nature Genetics, 25(4), 423–426. 10.1038/78113 [PubMed: 10932187]

Wang H, Hetmanski JB, Ruczinski I, Liang KY, Fallin MD, Redett RJ, … Beaty TH (2012). ROR2 gene is associated with risk of nonsyndromic cleft palate in an Asian population. Chinese Medical Journal, 125(3), 476–480. [PubMed: 22490406]

Watkins SE, Meyer RE, Strauss RP, & Aylsworth AS (2014). Classification, epidemiology, and genetics of orofacial clefts. Clinics in Plastic Surgery, 41(2), 149–163. 10.1016/j.cps.2013.12.003 [PubMed: 24607185]

Weiss JN, Karma A, MacLellan WR, Deng M, Rau CD, Rees CM, … Lusis AJ (2012). "Good enough solutions" and the genetics of complex diseases. Circulation Research, 111(4), 493–504. 10.1161/CIRCRESAHA.112.269084 [PubMed: 22859671]

Wittkowski KM, Sonakya V, Song T, Seybold MP, Keddache M, & Durner M (2013). From single-SNP to wide-locus: Genome-wide association studies identifying functionally related genes and intragenic regions in small sample studies. Pharmacogenomics, 14(4), 391–401. 10.2217/pgs.13.28 [PubMed: 23438886]

Yamaguchi TP, Bradley A, McMahon AP, & Jones S (1999). A Wnt5a pathway underlies outgrowth of multiple structures in the vertebrate embryo. Development, 126(6), 1211–1223. [PubMed: 10021340]

Yang Y, Topol L, Lee H, & Wu J (2003). Wnt5a and Wnt5b exhibit distinct activities in coordinating chondrocyte proliferation and differentiation. Development, 130(5), 1003–1015. 10.1242/dev.00324 [PubMed: 12538525]

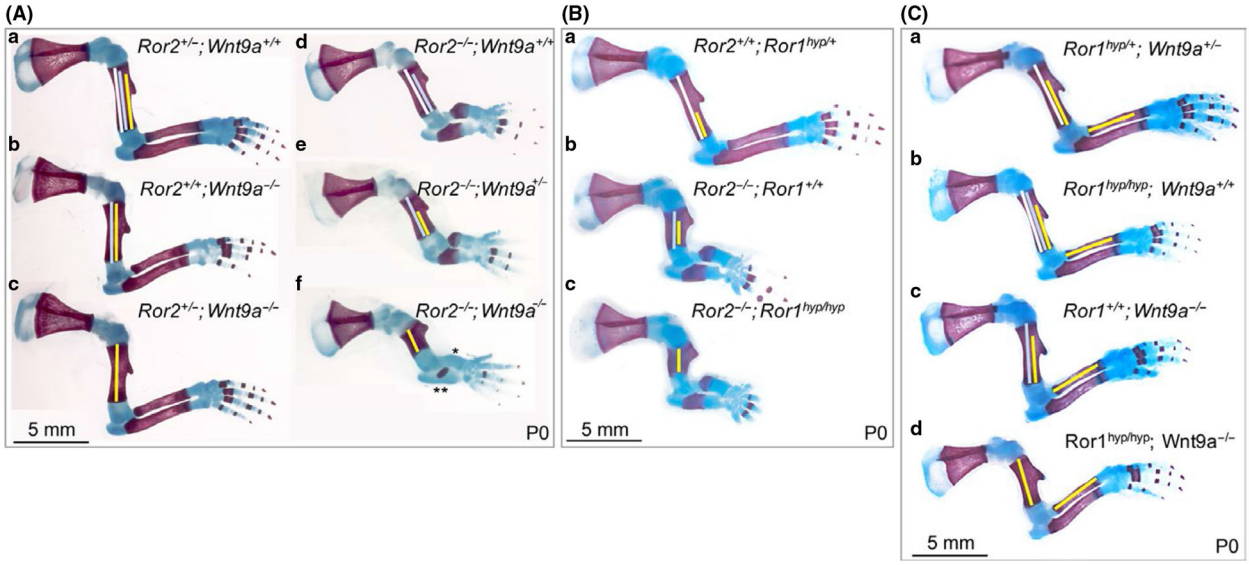

FIGURE 1.

Alizarin red/alcian blue-stained forelimbs of compound *Ror2;Wnt9a*, *Ror2;Ror1^{hyp}* and *Ror1^{hyp};Wnt9a* mutant newborn (P0) mice. (A) Successive shortening of the mineralized region of the ulnae upon loss of *Wnt9*a in a *Ror2* heterozygous (a–c) and *Ror2* homozygous mutant backgrounds (d–e). For comparison between the different genotypes, the length of the mineralized zone of the *Ror2$^{+/-}$;Wnt9a$^{-/-}$* mutant ulna is depicted by the yellow line in (a–c) and of the *Ror2$^{-/-}$;Wnt9a$^{-/-}$* ulna by the yellow line in (d–e), respectively. The light gray line in (a, b) depicts the length of the mineralized zone of the *Ror2$^{+/+}$;Wnt9a$^{-/-}$* ulna (b). The white line in (a) depicts the length of the mineralized zoneof the *Ror2$^{+/-}$;Wnt9a$^{+/+}$* ulna. The light gray line in (d, e) depicts the length of the mineralized zone of the *Ror2$^{-/-}$;Wnt9a$^{+/-}$* ulna (e). The white line in (d) depicts the length of the mineralized zone of the *Ror2$^{-/-}$;Wnt9a$^{+/+}$* ulna. (B) Successive shortening of the mineralized ulna region in *Ror2;Ror1^{hyp}* compound mutant newborn mice. The mineralized region of the ulnae is extremely small in the *Ror2$^{-/-}$;Ror1$^{hyp/hyp}$* double mutant (depicted by the yellow line in (c) compared to the size of this domain in *Ror2$^{-/-}$;Ror1$^{+/+}$* (gray line in (b)) and controls (*Ror2$^{+/+}$;Ror1$^{hyp/+}$*, white line in (a)). (C) Successive shortening of the mineralized region of the ulnae in *Ror1^{hyp}*; *Wnt9a* compound mutant newborn mice. For comparison, the mineralized regions of the ulna and the radius of the *Ror1$^{hyp/hyp}$;Wnt9a$^{-/-}$* double mutant (d) are depicted by the yellow lines for the ulna in (a–c) and for the radius in (a–d). The gray line in (a–c) depicts the length of the mineralized region of the *Ror1$^{+/+}$;Wnt9a$^{-/-}$* ulna, and the white lines in (a, b) depict the length of the mineralized region of the *Ror1$^{hyp/hyp}$;Wnt9a$^{+/+}$* ulna in (b) and the *Ror1$^{hyp/+}$;Wnt9a$^{+/-}$* ulna in (a), which do not differ. Size bars: 5 mm

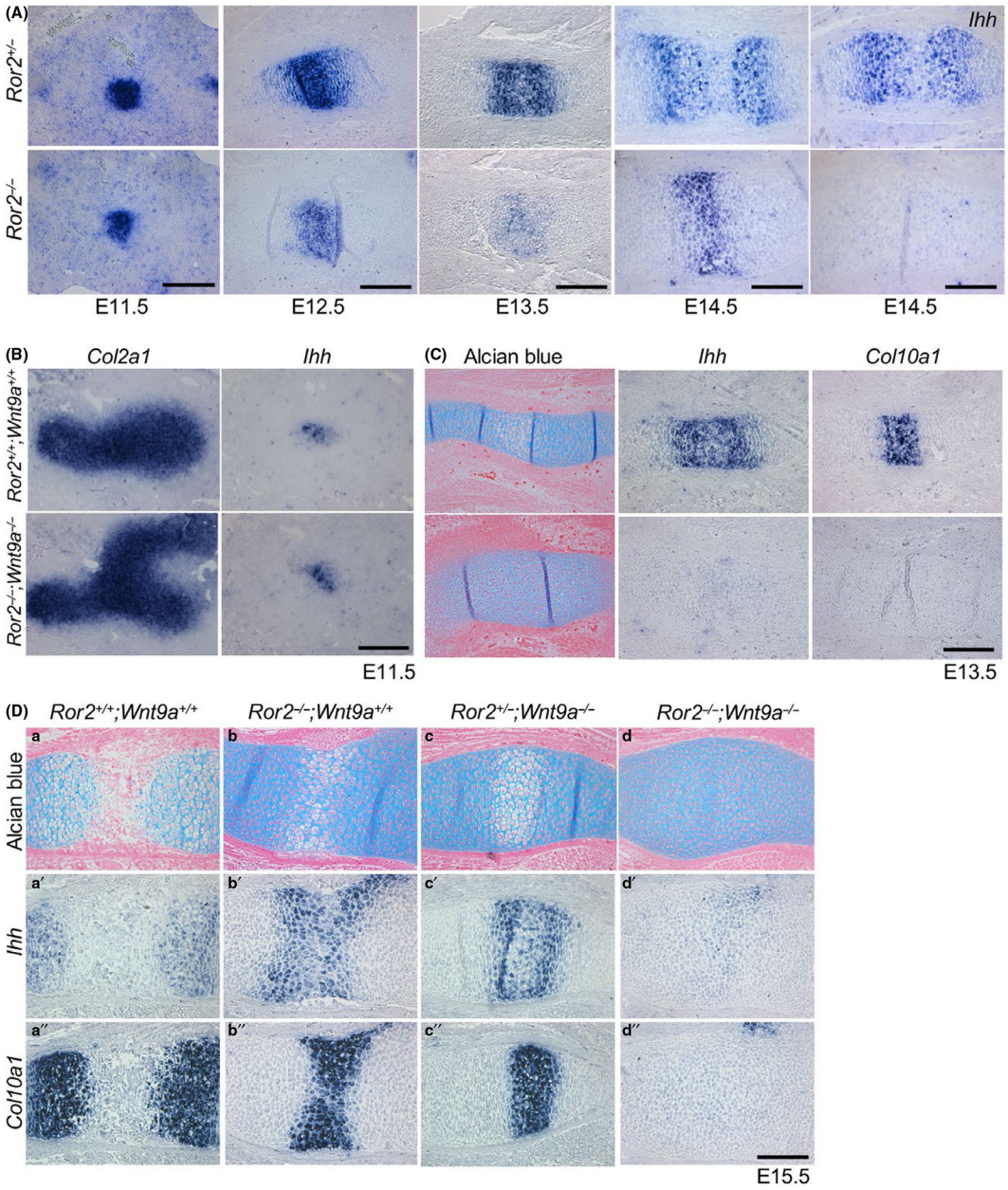

FIGURE 2.

Marker analyses (in situ hybridization) and histological examination of *Ror2* mutant and *Ror2;Wnt9a* compound mutant forelimb skeletal elements at different developmental stages. (A) Examination of the *Ihh* expression in the ulnae of $Ror2^{+/-}$ and $Ror2^{-/-}$ specimens at E11.5–E14.5. Note: From E12.5 onward, the *Ihh* domain is smaller in the $Ror2^{-/-}$ mutant specimens. In addition, at E12.5 and E13.5 the relative expression levels are decreased, and at E14.5, in half of the analyzed mutants (2/4) no *Ihh* expression is detected. Size bars: 200 μm. (B) *Col2a1* and *Ihh* expression in $Ror2^{-/-};Wnt9a^{-/-}$ double mutant compared to controls at E11.5. Serial sections through the forelimb. Note: The Col2a1 expression pattern looks different due to differences in the orientation of the limbs and the level of the section. The onset of *Ihh* expression in the ulna occurs normally in the $Ror2^{-/-};Wnt9a^{-/-}$ double

mutants. Size bars: 200 μm. (C) Histology, *Ihh* and *Col10a1* expression in *Ror2*$^{-/-}$;*Wnt9a*$^{-/-}$ double-mutant ulnae compared to controls at E13.5. Serial sections through the ulnae regions. Note: Absence of hypertrophic cells in the alcian blue-stained *Ror2*$^{-/-}$;*Wnt9a*$^{-/-}$ section. *Ihh* and *Col10a1* expression domains are also absent in sections through the *Ror2*$^{-/-}$;*Wnt9a*$^{-/-}$ mutant ulna. Size bars: 200 μm. (D) Comparison of *Ror2*$^{+/+}$;*Wnt9a*$^{+/+}$ (control, a–a″), *Ror2*$^{-/-}$;*Wnt9a*$^{+/+}$ (b–b″), *Ror2*$^{+/-}$;*Wnt9a*$^{-/-}$ (c–c″) and *Ror2*$^{-/-}$;*Wnt9a*$^{-/-}$ (d–d″) mutant specimens on serial sections through the ulnae regions at the level of histology (alcian blue staining), *Ihh* and *Col10a1* expression (in situ hybridization) at E15.5. Note the hypertrophic zone has not separated in the *Ror2*$^{-/-}$;*Wnt9a*$^{+/+}$ (b), *Ror2*$^{+/-}$;*Wnt9a*$^{-/-}$ (c) mutants and is absent in the *Ror2*$^{-/-}$;*Wnt9a*$^{-/-}$ (d) mutant. The *Ihh* domains are just beginning to split up in the *Ror2*$^{-/-}$;*Wnt9a*$^{+/+}$ (b′) and *Ror2*$^{+/-}$;*Wnt9a*$^{-/-}$ (c′) mutants, whereas barely any *Ihh* expression is detected in the *Ror2*$^{-/-}$;*Wnt9a*$^{-/-}$ (d′) mutant. The Col10a1 domains have not separated yet in the *Ror2*$^{-/-}$;*Wnt9a*$^{+/+}$ (b″) and *Ror2*$^{+/-}$;*Wnt9a*$^{-/-}$ (c″) mutants, and no *Col10a1* expression is detected in the *Ror2*$^{-/-}$;*Wnt9a*$^{-/-}$ (d″) mutant. Size bars: 200 μm

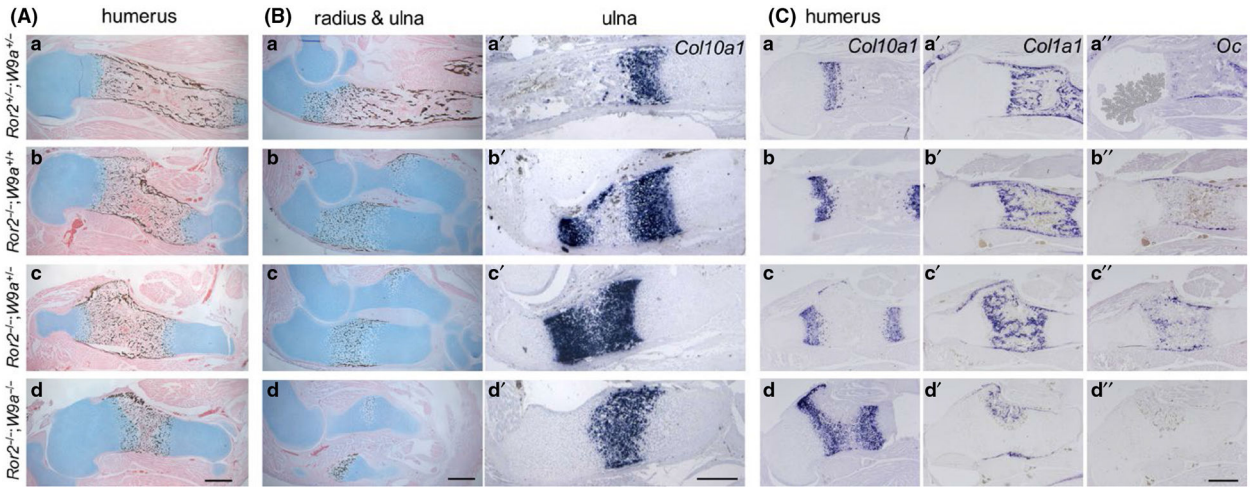

FIGURE 3.

Histology and marker analyses (in situ hybridization) of *Ror2;Wnt9a* compound mutant forelimb skeletal elements at P0. Note: For space reasons, Wnt9a is here abbreviated W9a. (Aa–d) von Kossa/alcian blue staining of humeri of the respective genotypes. Note: The mineralized region becomes successively smaller upon additional loss of *Wnt9a*. (Ba–d) von Kossa/alcian blue staining of radii and ulnae of the respective genotypes. Note: Bone marrow formation is severely compromised in *Ror2* mutants (b) and additional loss of one (c) or two (d) *Wnt9a* alleles delays the separation of the zones of maturated hypertrophic chondrocytes even further (c, c′) and further delays their maturation, reflected by the diminished mineralization (d). (Ca-d″) In situ hybridizations on serial sections through the humeri of *Ror2;Wnt9a* compound mutants for the hypertrophic marker *Col10a1* (a–d), the marker for osteoblasts *Col1a1* (a′–d′) and the marker for mature osteoblasts *Oc* (a″–d″). Note: Bone collar and trabecular bone formation are severely affected in the $Ror2^{-/-};Wnt9a^{-/-}$ double-mutant humerus, as *Col1a1* is diminished and *Oc* staining is absent in these humeri. Size bars: 500 μm

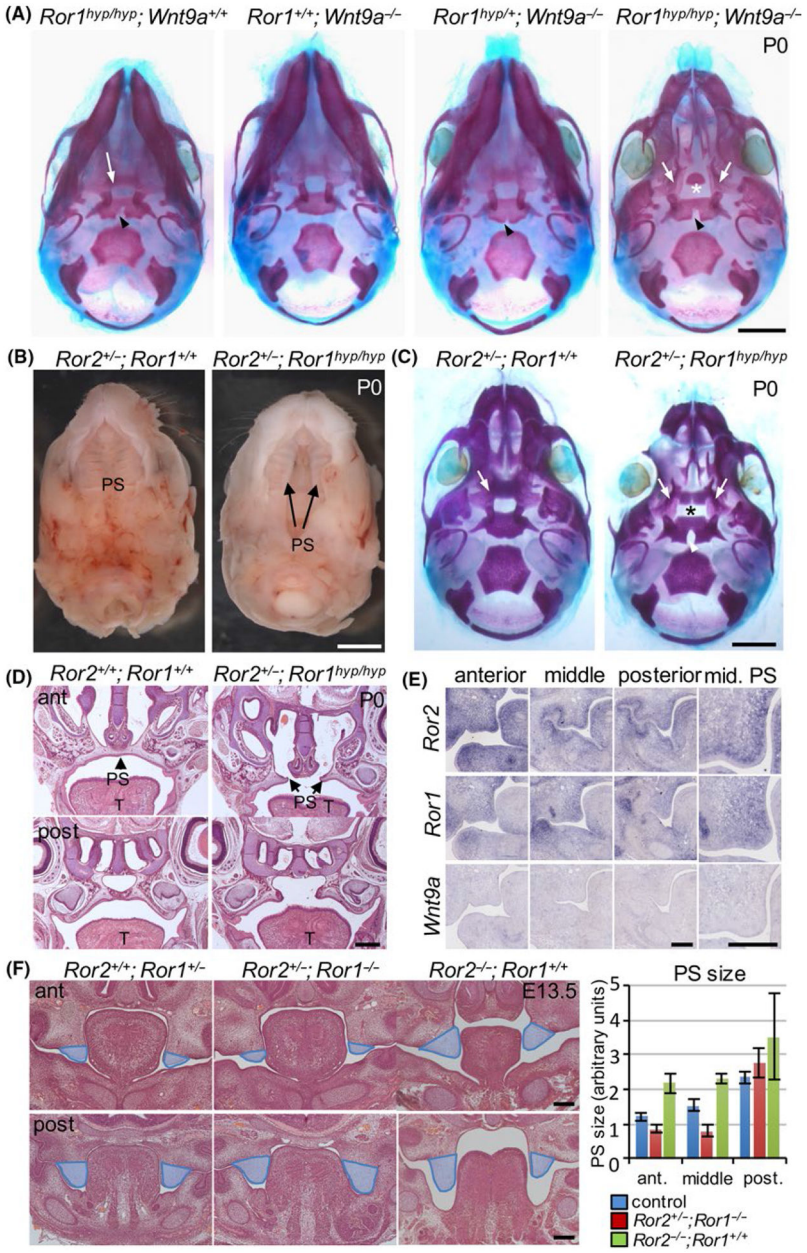

FIGURE 4.

Cleft secondary palate phenotype in *Ror1*^{hyp}/*Wnt9a* mutants and compound *Ror2/Ror1* mutant specimens. (A) View onto the cranial base of alizarin red (bone and mineralized tissue)/alcian blue (cartilage)-stained skulls of newborn (P0) *Ror1*^{hyp}/*Wnt9a* compound mutant mice. The nose is toward the top. Note: normal secondary palate development in *Ror1*$^{hyp/hyp}$;*Wnt9a*$^{+/+}$, *Ror1*$^{+/+}$;*Wnt9a*$^{-/-}$ and *Ror1*$^{hyp/+}$;*Wnt9a*$^{-/-}$ specimens (arrow). In *Ror1*$^{hyp/hyp}$;*Wnt9a*$^{+/+}$ and *Ror1*$^{hyp/+}$;*Wnt9a*$^{-/-}$, a cleft is present at the posterior base of the basisphenoid bone (arrowhead). A cleft secondary palate (white arrows) is visible in the *Ror1*$^{hyp/hyp}$;*Wnt9a*$^{-/-}$ mutant (note: here the lower jaw has been removed). In addition, a cleft is visible at the posterior end of the basisphenoid bone and the presphenoid bone has a different shape (white asterisk). (B) Whole-mount view of the palate of newborn

Ror2$^{+/-}$;*Ror1*$^{+/+}$ and *Ror2*$^{+/-}$;*Ror1*$^{hyp/hyp}$ specimens. The nose is toward the top, the lower jaw has been removed. PS: palatal shelf. (C) View onto the cranial base of alizarin red (bone and mineralized tissue)/alcian blue (cartilage)-stained skulls of newborn (P0) *Ror2*$^{+/-}$;*Ror1*$^{+/+}$ and *Ror2*$^{+/-}$;*Ror1*$^{hyp/hyp}$ mutant mice. The nose is toward the top. Note a cleft secondary palate (white arrows) is visible in the *Ror2*$^{+/-}$;*Ror1*$^{hyp/hyp}$ mutant specimen. A cleft is visible at the posterior edge of the basisphenoid (white arrowhead) and the presphenoid (black asterisk) bones. Size bars in a–c: 1 mm. (D) Hematoxylin/eosin-stained coronal sections through the anterior (ant) and posterior (post) regions of P0 heads of *Ror2*$^{+/+}$;*Ror1*$^{+/+}$ and *Ror2*$^{+/-}$;*Ror1*$^{hyp/hyp}$ specimens. The palatal shelves have not fused in the *Ror2*$^{+/-}$;*Ror1*$^{hyp/hyp}$ specimen. T: tongue; PS: palatal shelf. Size bar: 500 μm. (E) In situ hybridization with *Ror2*, *Ror1* and *Wnt9a* riboprobes on alternating coronal sections through an E13.5 head proceeding from the anterior to the posterior region. T: Tongue. Size bars: 250 μm. (F) Hematoxylin/eosin-stained coronal sections through the anterior (ant) and posterior (post) regions of E13.5 *Ror2*$^{+/+}$;*Ror1*$^{+/-}$, *Ror2*$^{+/-}$;*Ror1*$^{-/-}$ and *Ror2*$^{-/-}$;*Ror1*$^{+/+}$ mutant heads. Size bars: 200 μm. The palatal shelf area is colorized blue and quantified in the bar graph on the right side ($n = 2$; error bars are $\pm SD$). Quantification was carried out using ImageJ (area measurement)

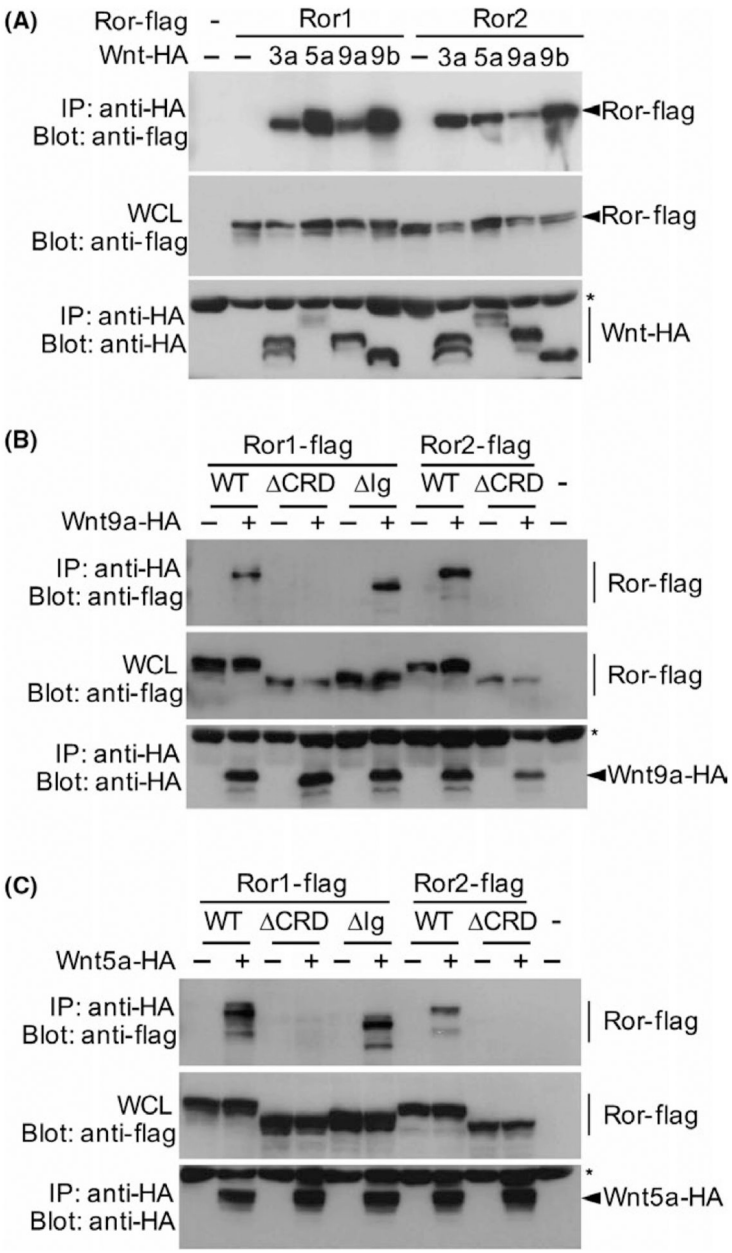

FIGURE 5.

Co-immunoprecipitation (Co-IP) blots for wild-type (WT) or mutant Ror-Flag and Wnt-HA-tagged proteins. (A) Co-IP for WT Ror1-Flag and WT Ror2-Flag with HA-tagged Wnt3a, Wnt5a, Wnt9a and Wnt9b. (B) Co-IP for flagged versions of WT-Ror1, Ror1 lacking the cysteine-rich domain (ΔCRD) or the Ig domain (ΔIg) and WT-Ror2 and Ror2ΔCRD in the absence or presence of an HA-tagged Wnt9a molecule showing interaction of Wnt9a with the WT-Ror1, ΔIg-Ror1 and WT-Ror2 molecules but lack of interaction with the ΔCRD versions of the Ror receptors. (C) The antibodies used for IP and the blot are indicated on the left side. WCL: Whole cell lysate showing the input signal of the Ror receptor proteins. The unspecific IgG background signal observed in the bottom blots is labeled by the asterisk